Influence of citric acid linker molecule on photovoltaic performance of CdS quantum dots-sensitized TiO$_2$ solar cells

G K R SENADEERA[1,2,]* **, W I SANDAMALI[1,2], M A K L DISSANAYAKE[2], T JASEETHARAN[2,3], V P S PERERA[1], J C N RAJENDRA[1], N KARTHIKEYAN[1] and LAHIRU A WIJENAYAKA[4]**

[1]Department of Physics, The Open University of Sri Lanka, Nawala, Nugegoda 10250, Sri Lanka
[2]National Institute of Fundamental Studies, Kandy 20000, Sri Lanka
[3]Department of Physical Sciences, Faculty of Applied Sciences, South Eastern University of Sri Lanka, Sammanthurai 32200, Sri Lanka
[4]Department of Chemistry, The Open University of Sri Lanka, Nawala, Nugegoda 10250, Sri Lanka
*Author for correspondence (gksen@ou.ac.lk)

Abstract. Influence of citric acid on the photovoltaic properties of the CdS quantum dot-sensitized TiO$_2$ solar cells (QDSSCs) was studied. Tethering of citric acid molecules with both TiO$_2$ and CdS quantum dots (QDs) was confirmed by Fourier transform infrared spectroscopy technique. High-resolution transmission electron microscopic studies revealed that QDs with average size of $\sim$4.5 nm, were tethered with TiO$_2$ nanoparticles of diameter $\sim$40 nm. Presence of Cd, S, C, Ti and O elements in the composite photoanode and their uniform distribution throughout the photoanode were confirmed by energy dispersive X-ray spectroscopy measurements. QDSSCs fabricated with pristine TiO$_2$ photoanode exhibited a short circuit current density (J_{SC}) of 5.80 mA cm^{-2} and an overall power conversion efficiency (η) of 1.10%, whereas solar cells made with citric acid-treated, photoanode-exhibited a J_{SC} of 8.20 mA cm^{-2} with 1.50% efficiency under 100 mW cm^{-2} (AM 1.5) light illumination. This is an impressive 60% increase in the J_{SC} and $\sim$36% enhancement in the overall power conversion efficiency. Interfacial resistance of QDSSCs is estimated by using electrochemical impedance spectroscopy revealed that citric acid treatment enhanced both the electron injection to the conduction band of the TiO$_2$ from the CdS as well as the overall charge transfer of the device, while decreasing the recombination of the photo-generated electrons with their holes in the electrolyte.

Keywords. CdS capping; quantum dots (QDs); citric acid; sensitization; solar cells.

1. Introduction

Nano particulate quantum dots (QDs) with diameters of <10 nm have been receiving widespread attraction in the recent past, due to their unique properties, such as size-dependent band gaps with broad excitation range, excellent chemical stability and high molar extinction coefficient [1]. Due to these properties, QDs could act as both photon harvesters (sensitizers) and tailor-made electronic transporting materials for dye-sensitized solar cells (DSSCs) [2–4]. Moreover, it is also believed that expensive silicon photovoltaic cells could be replaced with photovoltaic solar cells fabricated with QDs due to their lower manufacturing cost and the usage of simple techniques involved in the fabrication process compared to silicon solar cells [5]. Even though significant research studies have been performed on these QD-sensitized solar cells (QDSSCs), still their photochemical physics is not fully understood. Moreover, the power conversion efficiencies (η) of these QDSSCs without any modifications are generally much lower than the

DSSCs. To achieve high efficiencies in QDSSCs, the QDs have to be properly adhered to the TiO$_2$ nanocrystalline semiconducting photoanode surface, while having efficient pathways for photo-generated electrons or holes to be extracted from QDs before they recombine. In this context, linker or ligand-assisted assembly method where some molecules are used to tether the already synthesized QDs to the surfaces of the substrates [6] have been introduced. It is obvious that by this strategy, QDSSCs with higher efficiencies can be obtained with these photoanodes due to higher surface density coverage of QDs on the oxide substrate. The linker-assisted assembly is favoured with excellent properties because of extra ligands on the surface compared to the direct attachment of QDs to the semiconducting surface which provides inferior contact between QDs and semiconducting substrate [6,7]. However, the tethering of QD sensitizers on semiconducting surfaces has been a bottleneck in the development of efficient QDSSCs. In this context, CdS and CdSe QDs have been successfully tethered with TiO$_2$ using bifunctional linker molecules

(HOOC–RSH) comprising of carboxylic and thiol functional groups which facilitate the binding between the TiO_2 and the QD [7–18]. In particular, substantial work has been reported on CdSe tethered to TiO_2 via 3-mercaptopropionic, thioglycolic and cysteine [8], and mercaptopropionic acid (MPA) [15], 4-mercaptobenzoic acid, 3 thiophene carboxylic acid [17]. However, compared to CdSe, even though several studies have been carried out on the electron transfer between CdSe and TiO_2 via linkers, little work has been reported on QD solar cells fabricated with CdS tethered to TiO_2 via linkers [19–24]. For example, Wei *et al* [21] in 2015 reported that CdS-sensitized solar cells with thioglycolic acid linker having $\sim 0.45\%$ efficiency using nano rod arrays of TiO_2 and in subsequent work in 2017 by Yu *et al* [23] reported that QDSSCs fabricated with CdS QDs anchored on to TiO_2 nanotubes via different linker molecules including thioglycolic acid (TGA), mercaptopropionic acid (MPA) and cysteine via hydrothermal method exhibited overall efficiencies of 1.49, 0.82 and 2.16%, respectively. In another study, Razzaq *et al* [22] have obtained an efficiency enhancement from 0.18 to 0.38% by using 2-mercaptoethanol (ME) as the linker in these devices. A bifunctional surface modifier, 3-mercaptopropyl trimethoxysilane (MPTMS) used by Lin *et al* [25] have reported solar cells with 1.35% efficiency. However, most of the reported CdS-sensitized TiO_2-based solar cells with different linker molecules show efficiencies <1.5%. One of the reasons for these lower efficiencies could be very likely due to the difference in the interfacial environments owing to the nature of the linker molecule used in these methods which leads to the poor tethering of QDs into the oxide matrix with irregular surface loading of QDs on the semiconducting substrates [21,23]. However, in this context, according to our knowledge, naturally abundant, simple molecule, citric acid which is formed by the tricarboxylic acid cycle [26], has not been used previously as a linker to attach CdS especially with the semiconductor TiO_2. Citric acid is an important surface ligand in the preparation of a wide range of nanomaterials which can be used in various applications, such as sensors and biomedical devices. The carboxylate groups in citric acid have the ability to coordinate with TiO_2 as well as with Ti ions [26,27]. This coordination is one of the most important aspects in efficient photo-generated electron transfer to the conduction band of the semiconductor from QD. This linkage is very similar to the organic dye molecules with intimate interfacial contacts with TiO_2 benefitting the photo-generated electron injection. Moreover, as in the DSSCs, availability of this carboxyl ions (COO^-) could prevent the formation of multilayers of QDs on the semiconductor. On the other hand, since the citric acid possesses shorter chain lengths with smaller inter-particle distances than other available linkers, one can expect faster electron transfer from the QD to the semiconductor. Hence, literally, citric acid should be one of the best linkers for these QDSSCs. Therefore, by considering all these factors, for the

first time, in the present study, we have demonstrated the possibility of using citric acid successfully as a linker molecule and a capping agent in the fabrication of CdS QDSSCs. To realize the better performance of QDSSCs, a combination of the linker-assisted assembly with successive ionic layer adsorption and reaction (SILAR) method has been implemented. The SILAR cycles were initiated with immersion of citric acid-treated TiO_2 electrodes in Cd^{2+} precursor solution and subsequently, immersing in the S^{2-} solutions. Reasonably, high power conversion efficiency was achieved by this simple technique compared to the conventional QDSSCs made without any modifications of the photoanode material as well as to the devices fabricated with other linkers [25–27].

2. Experimental

2.1 *Preparation of TiO_2 photoanode*

To minimize the short circuiting of the solar cells, at first, compact layer (CL) of TiO_2 was deposited by spin-coating titanium (IV) isopropoxide precursor solution (97%, Fluka) on a pre-cleaned, fluorine-doped, tin oxide (FTO) glass substrate ($8 \ \Omega \ cm^{-2}$, Solarnoix), for 1 min at 3000 rpm. The substrate was then sintered at 450°C for 45 min and cooled down to room temperature. To decrease the electron recombination in the DSSC, another compact layer of TiO_2 was spin-coated on above substrate by using a paste prepared with 0.25 g of TiO_2 P90 powder (Evonik, 90% anatase, 10% rutile) and 1 ml of HNO_3 (70%, Sigma-Aldrich). Spin coating of this layer was done for 1 min at 3000 rpm. The spin-coated substrate was again sintered at 450°C for 45 min. Subsequently, a coating of TiO_2 P25 (Degussa, 85% anatase, 15% rutile), active layer was 'doctor bladed' on the P90 layer of the above substrate by using a mixture of 0.25 g of TiO_2 P25 powder, 1 ml of 0.1 M HNO_3, 0.05 g of polyethylene glycol (99.8%, Sigma-Aldrich) and 1 drop of triton X-100 (Sigma-Aldrich). Finally, the substrates with all three TiO_2 layers were again sintered at 450°C for 45 min and allowed to cool down to room temperature.

2.2 *Citric acid surface-modification of TiO_2 nanoparticles*

The aforementioned TiO_2 substrates with the FTO/CL/P90/P25 configuration were dipped in a citric acid (CA, monohydrated, 99.5%, Sigma-Aldrich) solution with 0.5 M citric acid in ethanolic medium (99.8%, Sigma-Aldrich), for different dipping times. The optimum dipping time was obtained by fabricating and testing solar cells with configuration FTO/TiO_2/CA/CdS/electrolyte/Pt/FTO as mentioned below. Solar cells with the highest efficiency were obtained from the photoanodes treated with 1 h dipping in CA solution. Attenuated total reflection infrared (ATR-IR)

spectra of the citric acid and the citric acid-adsorbed TiO_2 substrates were obtained using a Nicolet iS50 (Thermo Scientific) FTIR instrument.

2.3 *Sensitization of TiO_2 photoanode with CdS QDs*

Sensitization of TiO_2 photoanode (FTO/CL/P90/P25) with CdS QDs was done by using a ligand-assisted successive ionic layer adsorption and reaction (SILAR) method. The CdS QDs were deposited on the citric acid-treated TiO_2 photoanode by 10 SILAR cycles [3,4], one cycle consisting of dipping the photoanode in cationic precursor solution for 1 min, washing with distilled water, drying in air, again dipping in anionic precursor solution for 1 min, washing with distilled water and finally, drying in air. Aqueous solutions of 0.1 M $CdCl_2$ (99.99%, Sigma-Aldrich) and 0.1 M Na_2S (mono hydrated, 60%, Sigma-Aldrich) were used as cationic and anionic precursor solutions, respectively. Finally, the photoanodes were dried at different temperatures and optimized temperature was selected by fabricating and testing solar devices. Optimized drying condition was found to be 40 min at 100°C. A reference CdS-sensitized photoanode was prepared by following the same SILAR process for a non-citric acid-treated TiO_2 photoanode. Schematic diagram showing tethering of CdS on TiO_2 via CA is depicted in figure 1.

2.4 *Fabrication of QDSSC*

CdS-sensitized TiO_2 photoanodes prepared with and without citric acid treatments having an effective area of

Figure 1. Schematic diagram of photoanode containing citric acid molecules attached with TiO_2 crystallites via the COO^- terminals.

0.25 cm^2 were sandwiched with Pt-coated FTO counter electrodes using steel clips and an appropriate amount of polysulphide electrolyte containing sulphide/polysulphide redox couple (S^{2-}/S_n^{2-}) prepared with sulphur (2 M, 99%, Daejng) and Na_2S (2 M) in a mixed solution of deionized water and methanol in the ratio of 3:7 (v/v).

2.5 *Characterization*

Fabricated FTO/TiO_2 photoanodes were characterized by the following techniques. The phase composition and crystallinity of the P90/P25 photoanode were determined using X-ray diffractometer (BTX compact Benchtop XRD system) with CuKα radiation (l = 0.1541 nm), high-resolution transmission electron microscopy (HRTEM) imaging was carried out with a JEOL JEM-2100 TEM at an accelerating voltage of 200 kV. Energy dispersive X-ray (EDX) spectra were obtained from Ametek EDX module with Octane T Optima-60 EDX detector in TEM mode. Diffuse reflectance UV–visible absorption spectra were measured by Shimadzu 2450 UV–VIS spectrophotometer. Attenuated total reflection infrared (ATR-IR) spectra were obtained using a Nicolet iS50 (Thermo Scientific) FTIR instrument. Current–voltage and impedance characterizations of fabricated QDSSC were carried out under simulated light of 100 mW cm^{-2} with AM 1.5 filter by using Autolab potentiostat/galvanostat PGSTAT128 N. To ensure the repeatability of the device performance, at least five solar cells from each type were fabricated and tested. Electrochemical impedance spectra (EIS) of CdS QDSSCs were obtained by using a frequency response analyzer (Metrohm) in the frequency between 0.01 Hz and 1 MHz under the same simulated light intensity at room temperature.
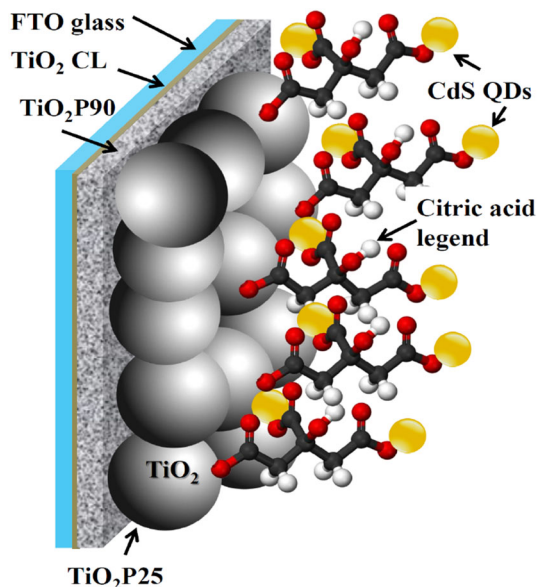
3. Results and discussion

3.1 *Phase composition and crystallinity of the photoanode*

To see the phase composition and crystallinity of the photoanode, XRD measurements were performed on the glass/FTO substrate and the glass/FTO/P90/P25. Figure 2 shows the XRD spectra of the glass/FTO/P90/P25 photoanode. As shown in the figure, the major XRD peaks correspond to the anatase (JCPDS card no. 21-1272) phase are found at 2θ values of 24.8, 37.3, 47.6, 53.5, 55.1, 62.2 and 75.5° corresponding to (101), (004), (200), (105), (211), (204) and (215) crystal planes. The peaks correspond to the rutile (JCPDS card no. 21-1276) phase are found to be at 2θ values of 27.0, 35.6, 41.8, 64.6, 68.5° corresponding to the crystal planes of (110), (101), (111), (210), (311), (220), (310) and (301) [28–30].

The phase composition in annealed photoanode with P90 and P25 layers estimated from the Spurr Meyers equation found to be 81% anatase and 19% rutile [28]. Therefore, the
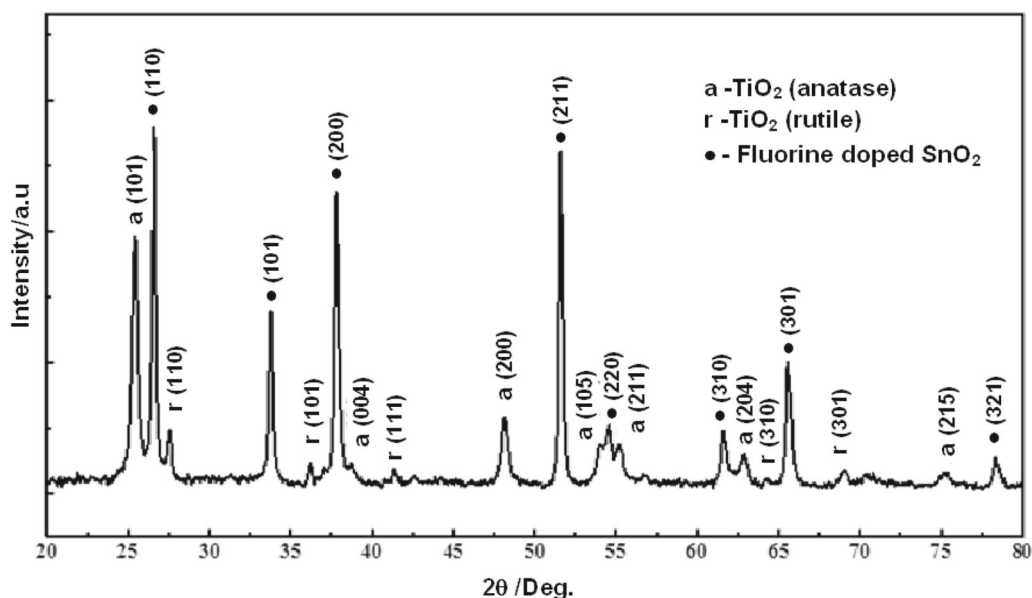
Figure 2. X-ray diffraction pattern of titanium dioxide phases of the photoanode configuration glass/ FTO/P90/P25: a, anatase TiO_2; r, rutile TiO_2; and •, SnO_2.
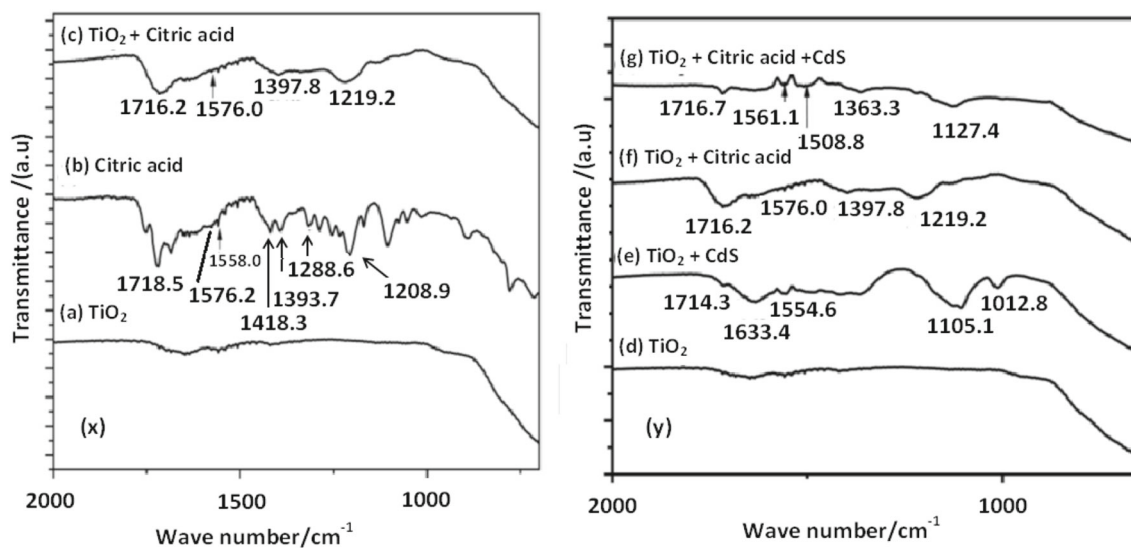

Figure 3. FTIR spectra of the electrodes containing: (**x**) (**a**) TiO_2, (**b**) citric acid, (**c**) TiO_2/citric acid and (**y**) (**d**) TiO_2, (**e**) TiO_2–CdS, (**f**) TiO_2-citric acid and (**g**) TiO_2–citric acid/CdS.

structure of the fabricated photoanode mainly consists of anatase phase of the TiO_2.

3.2 *FTIR analysis*

The functional groups of a molecule are important for the adsorption of the molecule to the semiconducting TiO_2 surface. We have used the citric acid monolayers as templates to deposit a CdS layer on the surface of TiO_2. The terminal carboxylic functional groups of the citric acid

facilitates the chemisorption of citric acid to the surface of TiO_2 which will lead to more uniform coating of CdS to the TiO_2 [26]. Figure 3x shows the FTIR spectra of (a) TiO_2, (b) citric acid and (c) citric acid-attached TiO_2. As shown in curve (b), the bands appeared near 1393 and 1570 cm^{-1} are assigned to asymmetric and symmetric stretching motions of the carboxylate groups, respectively. The prominent peak observed at 1718 cm^{-1} for citric acid (line b) is shifted to 1716 cm^{-1} and no longer it will be the most intense band in the spectrum (c). In agreement with the observations reported by Mudunkotuwa and Grassian [26] on citric acid

attachment on TiO$_2$, this band shifts towards the lower frequency direction arises most likely due to the interaction of TiO$_2$ with citric acid by weakening the C=O bond. Further, C–O stretching of carboxylic acid around 1320–1210 cm^{-1}, can be observed at 1208.9 cm^{-1} in citric acid and at 1219.2 cm^{-1} in citric acid-attached TiO$_2$. The weaker bond at 1280 cm^{-1} which is assigned to coupled stretches and bonds of the carboxylate group in the citric acid will no longer appear in the curve (c) due to the attachment between TiO$_2$ and citric acid. Similar to the FTIR observations reported by Mudunkotuwa and Grassian [26] on citric acid adsorption on TiO$_2$, bands appear in the spectrum can be assigned to the stretching as mentioned in table 1. Figure 3y shows the FTIR spectra for the QDs attachment to the TiO$_2$ citric acid. As can be seen from curve (f), the intensity of the band near 1716.2 cm^{-1} is further decreased due to possible interaction of CdS with citric acid C=O bond. The peak appearing at 1219 cm^{-1} for citric acid-treated QDs can be ascribed to the stretching vibration of the C–H group and indicate the presence of incompletely carbonized citric acid. The peak at 1127 cm^{-1} for citric acid arise from the –C–O–C group stretching vibration [26]. Therefore, it is clear that some of the CdS nanoparticles are moved to TiO$_2$ via citric acid. These observations correlated with the data published by Wang *et al* [31] on citric acid-capped CdS QDs. As reported by Cao *et al* [32], the interaction between COO– groups on CdS should lead to the formation of a well-combined interface, which should greatly promote the efficient transfer of electron–hole pairs and prolonged the lifetime of charge carriers generated by light absorbed by the CdS.

3.3 *EDX spectroscopy characterization*

Figures 4 and 5 show the EDX spectrum and the elemental mapping of the fabricated CdS QD-sensitized TiO$_2$ photoanodes, respectively. EDX analysis clearly shows the presence of Cd, S, C, Ti and O elements in the composite sample. The peaks which correspond to the C and O elements present in the figure must be attributed to the existence of the citric acid molecules.

Table 1. FTIR frequencies and assignments for citric acid-treated TiO$_2$ film.

Mode of vibration	Vibrational frequency (cm^{-1})
ν(C=O)	1716
ν_{as}(COO–)	1570
ν_s(COO–)	1397
ν(C–OH)	1094
ν(OC–OH)+	1219
δ(CH$_2$)	1436
δ(O=C–O–)	1292, 1262

The elemental mapping of synthesized CA–CdS QDs was carried out for analysing the element distribution. Figure 4 shows the element distribution of Cd, S and O in the photoanode. The results indicated that uniform distribution of Cd, S and O throughout the photoanode.

3.4 *Morphological characterization*

As it is well known that the CdS QDs are few nanometres in size. High resolution TEM (HRTEM) images were mainly used to analyse the microstructure and the particle size of the TiO$_2$/CdS surfaces with and without the citric acid treatment. Figure 6 shows the TEM images of both with citric acid (figure 6b) and without citric acid (figure 6a) treated TiO$_2$/CdS surfaces. Highly dense dispersion of CdS QDs in citric acid-treated TiO$_2$ matrix can be seen in figure 6b. Figure 6c shows the HRTEM image of the CdS QD-sensitized TiO$_2$ nanostructure. While the average size of the QDs appears to be in the 4.0–4.5 nm range, the size of the TiO$_2$ particles appears to be around 40 nm. This was further confirmed by the SEM image of the TiO$_2$ as shown in figure 6d. However, since the size of the QDs are in the range of 4.0–4.5 nm, it was confirmed only by HRTEM studies due to the resolution limitations of the SEM instrument. It can be seen from figure 6c that two types of lattice planes corresponding to the (101) plane of both CdS and TiO$_2$ with inter-planar distance of 0.31 and 0.35 nm. As it was reported by Kavil *et al* [33], this can be considered as ideal hybridization established between TiO$_2$ and CdS nanoparticles in TiO$_2$–CdS heterostructure with citric acid.

3.5 *UV–visible absorption*

Figure 7 shows the normalized diffuse reflectance UV–visible absorption spectra (Kubelka–Munk function *vs.* wavelength) of pristine (a) TiO$_2$, (b) CdS with TiO$_2$ and (c) CdS with CA-treated TiO$_2$. To minimize the contribution of light scattering to the baselines of absorption curves, diffuse reflectance UV–visible spectra were acquired. Diffuse reflection spectra of QD functionalized films correspond closely to those of dispersed QDs and did not exhibit interference fringes or sloping baselines. Because the path length in diffuse-reflectance measurements was unknown, we report *y*-axis of diffuse reflectance UV–visible spectra as apparent absorption $F(R)$, where R is the intensity of scattered light divided by the intensity of incident light [34]. According to the curve (a), the large band gap semiconductor TiO$_2$ crystallites with ~ 40 nm diameter confirmed by HRTEM, absorb the light in the UV region with an onset at ~ 380 nm which is in agreement with the band gap of anatase TiO$_2$ (3.2 eV). Curve (b) represents the light absorption of CdS on TiO$_2$ without CA treatments. As can be seen from the shoulder around the wavelength at 450 nm, the light absorption expanded from ultra violet light to
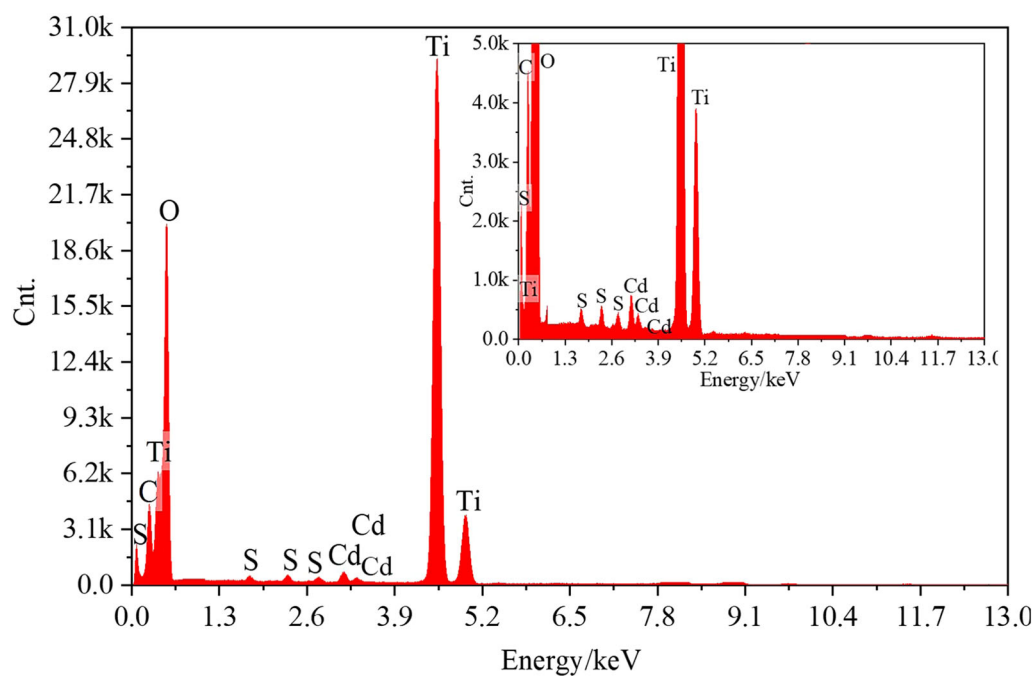
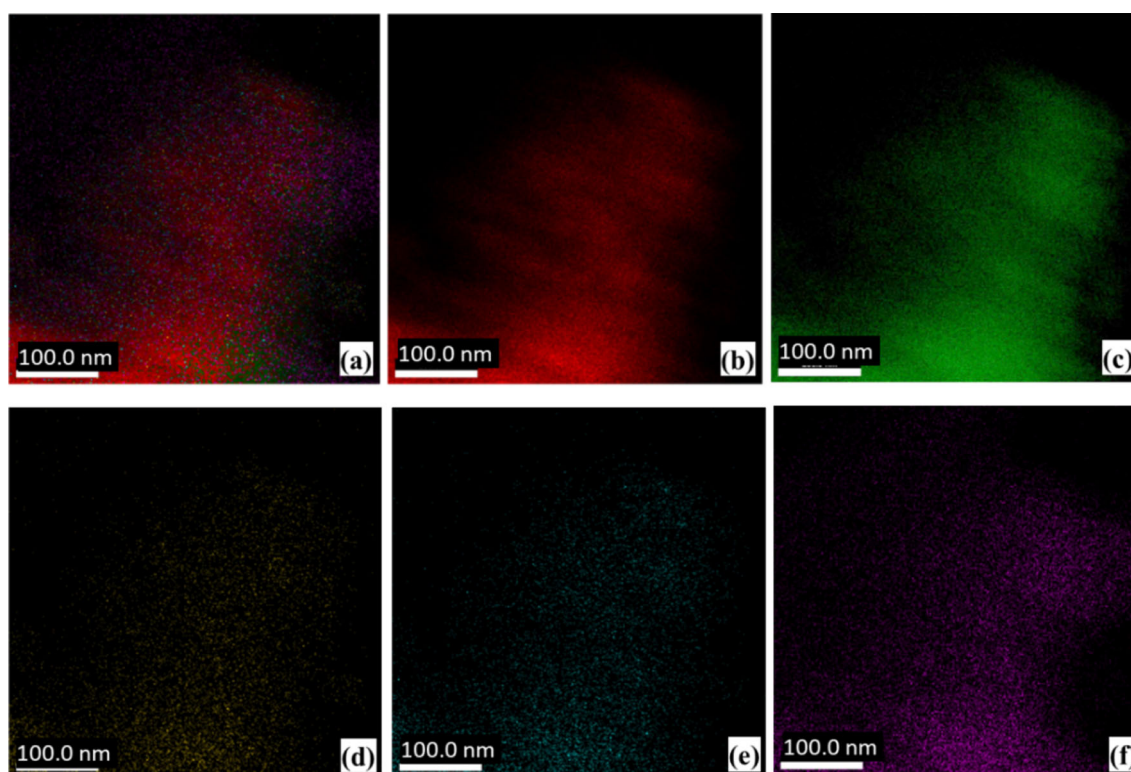**Figure 4.** EDX spectrum of CdS quantum dot-sensitized TiO_2 electrode.

Figure 5. Elemental mapping of (**a**) selected area, (**b**) Ti (51%), (**c**) O (17%), (**d**) Cd (1%), (**e**) S (1%) and (**f**) C (7%).

visible light region when CdS QDs are anchored onto the TiO_2. It can be clearly seen from the curves (b) and (c) after the introduction of citric acid, the total absorption of CdS on TiO_2 extends its absorption to the longer wavelength region. This red-shift can be considered as the evidence for different natures of the electronic coupling between CdS and
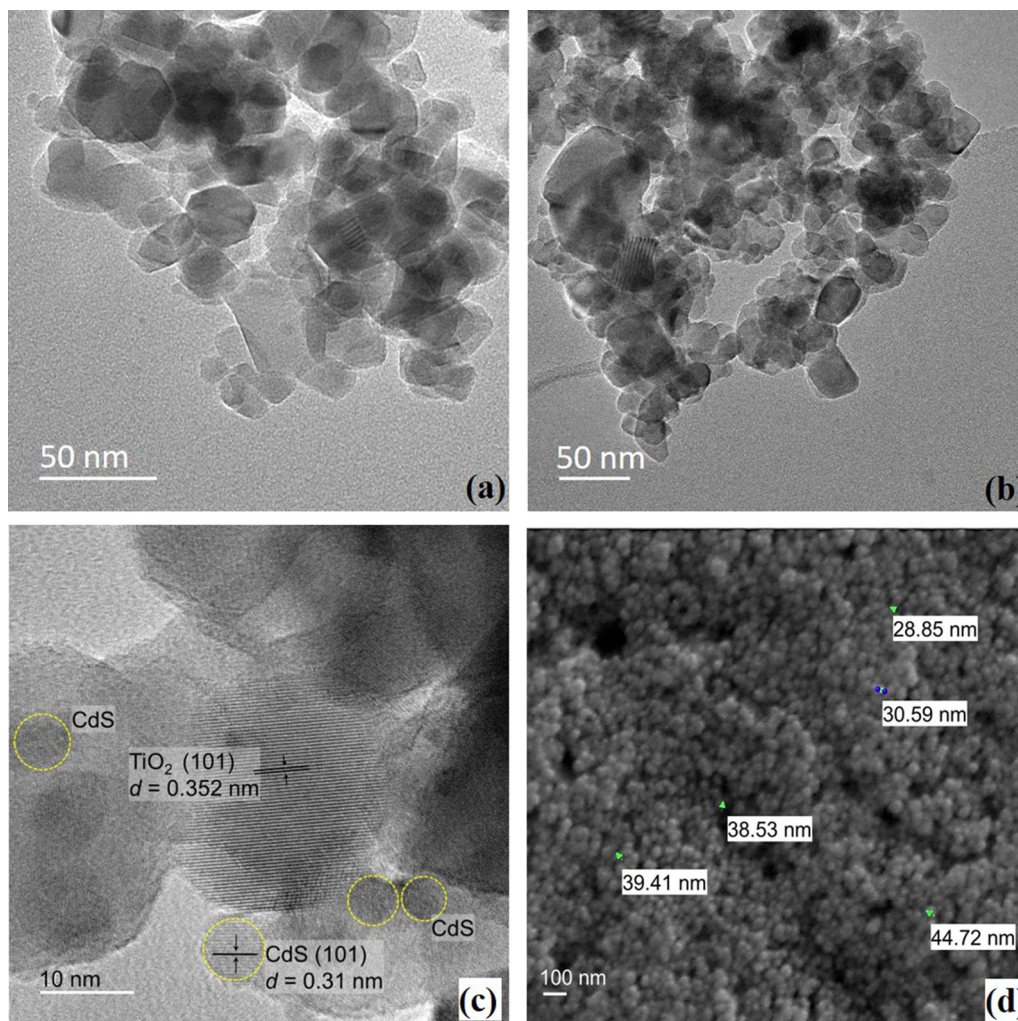
Figure 6. TEM images of CdS quantum dot-sensitized TiO_2 electrode: (**a**) without and (**b**) with citric acid treatment, (**c**) HRTEM image of CdS quantum dot-sensitized TiO_2 nanostructure and (**d**) SEM image of a TiO_2 surface.
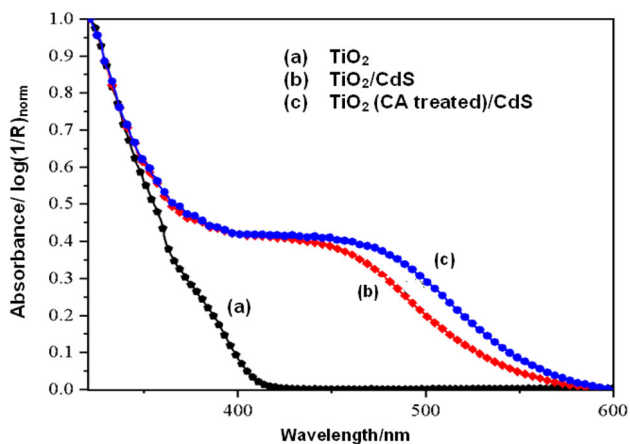

Figure 7. Diffuse reflection absorption spectra of (**a**) bare TiO_2, (**b**) TiO_2/CdS and (**c**) TiO_2/CA/CdS showing clear shift in absorbance towards red region with CA-treated TiO_2/CdS deposition.

TiO_2 [35] which is correlated with the results obtained in FTIR and TEM analyses.

3.6 *I–V characteristics of CdS QDSSCs*

Figure 8 shows the current density–voltage (J_{SC}–V) characteristic of QDSSCs fabricated with TiO_2 CdS-sensitized photoanodes (a) without and (b) with citric acid treatments comprising the sulphide electrolyte under a simulated AM 1.5 solar irradiation with a light intensity of 100 mW cm^{-2}. The area of all the devices was kept as 0.25 cm^2. As it is evident from the figure, significant enhancement can be seen in the photocurrent density (J_{SC}) of the device with CA-treated CdS/TiO_2 photoanode with a slight increase in the photovoltage. The values of the short-circuit-current density J_{SC}, the open-circuit voltage V_{OC}, the fill factor *FF* and the photovoltaic conversion efficiency η are estimated from figure 8 are tabulated in table 2. Power conversion
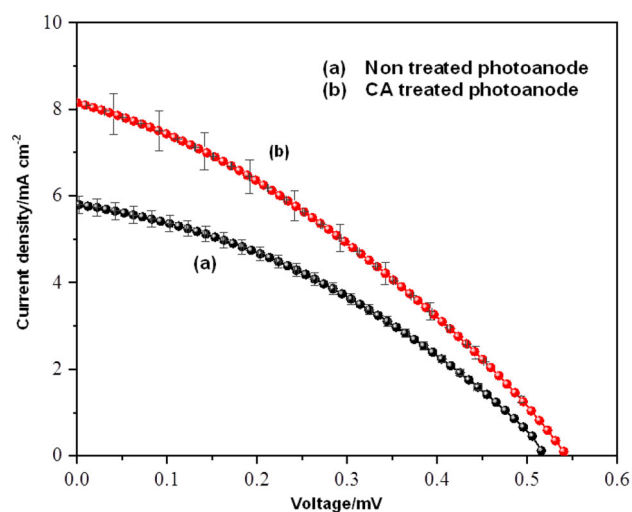
Figure 8. Current density–voltage characteristics of CdS QDSSCs fabricated with (**a**) untreated photoanode and (**b**) photoanode treated with citric acid, under the illumination of 100 mW cm^{-2} with AM 1.5 spectral filter.

efficiency of each QDSSC were calculated using the following equation [36]:

$$\eta = \frac{J_{SC} \cdot V_{OC} \cdot FF}{P_{IN}} \times 100\%,$$

where the symbols have their usual meaning and P_{IN} is the incident power density which is 100 mW cm^{-2}.

For both with and without CA treatments, the photovoltaic conversion efficiency η predominantly depends on the short-circuit-current density J_{SC}, as shown in table 2. On the other hand, slight increase in the V_{OC} can also be seen. As mentioned by Cho *et al* [37], this enhancement in V_{OC} could be due to the increase in the quasi-Fermi level in the TiO$_2$ with the increase in the density of the electrons injected from QDs. The overall power conversion efficiencies and J_{SC} values of the QDSSCs with and without citric acid-treated photoanodes under above light illuminations are ~1.5%, 8.2 mA cm^{-2} and 1.1%, 5.8 mA cm^{-2}, respectively. It should be mentioned here that as practiced by the DSSC community, after measuring a large number of solar cells of each type, these average values were chosen by considering the repeatability of the measurements though it was possible to get even much higher values for the efficiency for some cells than the reported average values. However, to maintain the clarity of the figure, only

two curves are shown for the comparison in figure 8. Corresponding deviations in solar cell parameters are given in table 2. Therefore, QDSSCs fabricated with CA-treated TiO$_2$ films shows nearly 52% increase in the J_{SC} values. The overall efficiency enhancement is ~36%. This enhancement could be due to the increased amount of QDs attached to the semiconductor surface with efficient transfer of photo-generated carriers between the QDs and TiO$_2$ particles as observed by others in the cases of oleic acid and tri-octylphosphine oxide (TOPO) ligands [38,39]. As it was reported by Yang *et al* [36] and Gopi *et al* [40], since Pt counter electrode is not a good electrocatalyst for the polysulphide redox electrolytes, much higher FF and higher photovoltaic conversion efficiencies can be expected by using copper sulphide counter electrodes which act as a better catalyst for the polysulphide redox reaction. However, it should be noted that the energy conversion efficiency of the CdS-sensitized solar devices fabricated with the present strategy is comparable and even higher than some of the efficiency values reported in the literature by using different strategies, such as doping with different materials [41,42] as well as usage of expensive linker material [24–27]. Therefore, it can be concluded that by using the COO– groups in the citric acid, significant enhancement in the efficiency of CdS-sensitized QDSSCs can be achieved by this simple, inexpensive and environmentally friendly linker method [40].

3.7 *EIS of CdS QDSSCs*

To see the effect of linker molecule on the enhancement of the photovoltaic performance, EIS measurements were carried out on the QDSSCs. Figure 9 shows the impedance spectra of CdS-sensitized solar devices fabricated with and without citric acid-treated photoanodes under the light conditions. This figure depicts two common main features for both the devices. Two semicircles are observed. The first semicircle in the high frequency region arises from the charge transfer resistance at the counter electrode/electrolyte interface coupled with the double layer charge capacitance. The second semicircle, at lower frequencies, exhibits the well-established semi-finite Warburg impedance relative to the diffusion control by redox mediator in the electrolyte at the TiO$_2$/QDs–electrolyte interface [3,4]. The series resistances (R_s) of the FTO/TiO$_2$ interface, the resistance of the counter electrode/electrolyte interface

Table 2. Photovoltaic parameters of CdS QDSSCs under the illumination of 100 mW cm^{-2} with AM 1.5 spectral filter.

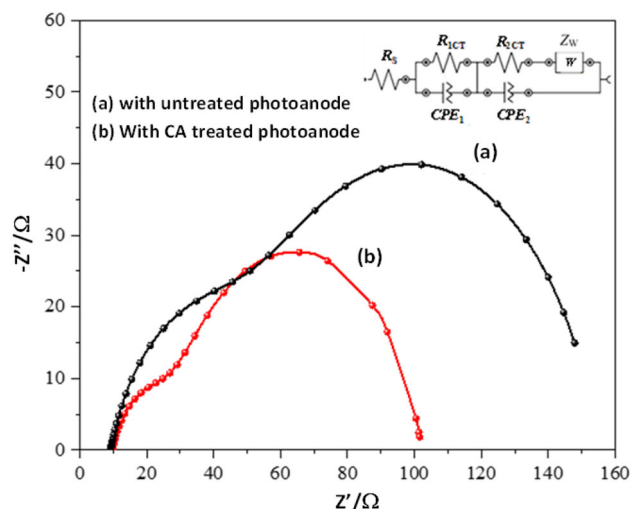| TiO$_2$ photoanode	J_{SC} (mA cm^{-2})	V_{OC} (mV)	FF (%)	Efficiency, η (%)
Untreated	5.8 ± 0.2	525 ± 5	36 ± 1	1.1 ± 0.1
Treated	8.2 ± 0.5	545 ± 2	33 ± 3	1.5 ± 0.2

Figure 9. Impedance spectra of CdS-sensitized solar cells fabricated with (**a**) untreated and (**b**) citric acid-treated photoanode, under the illuminated condition.

Figure 10. Schematic diagram of band positions of TiO_2 and CdS semiconductors and possible electron transfer mechanism.

Table 3. EIS parameters of CdS QDSSCs under the illumination of 100 mW cm^{-2} with AM 1.5 spectral filter.

TiO_2 photoanode	R_s (Ω)	R_{1CT} (Ω)	R_{2CT} (Ω)	Z_w (Ω)
Untreated	8.62	125	21.6	11.8
Citric-acid treated	6.90	46.8	43.4	23.4

(R_{1CT}) and the resistance of the photoanode/electrolyte (R_{2CT}) (recombination resistance) of these two devices were estimated by using the equivalent circuit as shown in the inset of the figure and estimated values are tabulated in table 3.

Constant phase elements related to the first interfaces are represented by CPE1 and CPE2. R_{3CT} is related to the finite Warburg impedance which originates from the difference of the diffusion coefficients of the positive and negative ions in the electrolyte as well as the non-blocking character of the electrodes [3,4]. As it is evident from the table, the series resistance R_s and the charge transfer resistance R_{1CT} of the QDSSC fabricated with citric acid-treated photoanode are lower than those of the device fabricated with untreated photoanode. On the other hand, the QDSSc fabricated with citric acid-treated photoanode shows much larger charge transport resistance (R_{2CT}) corresponding to the TiO_2/QDs–electrolyte interface. This change is obvious due to the presence of the linker molecule and the increase in R_{2CT} clearly depicts the increase in recombination resistance. Therefore, this clearly confirms that QDSSCs fabricated with citric acid-treated TiO_2 photoanode exhibit lower recombination rate at TiO_2/QDs–electrolyte interface. This phenomenon further confirmed and correlated with the significant enhancement of J_{SC} as well as the enhancement
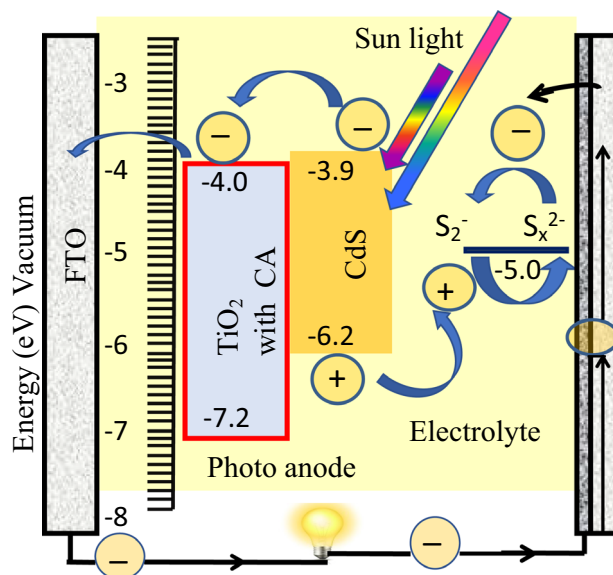
in the V_{OC} of the device fabricated with citric acid-treated photoanode. Therefore, citric acid molecules can facilitate the charge transfer rate from QDs to TiO_2 effectively due to the effect of COO− groups of citric acid, leading to the increment in J_{SC} and eventually, the efficiency of these devices [25]. The increase in V_{OC} can be explained by using the following equation as mentioned by Cho *et al* [37]:

$$V_{OC} = \frac{E_{Fn} - E_{Redox}}{e} = \frac{k_B T}{e} \ln\left[\frac{n}{n_o}\right],$$

where E_{Fn} is the quasi-Fermi level of the electrons in the semiconductor photoanode under illumination, E_{Redox} the potential of the redox electrolyte, e the positive elementary charge, $k_B T$ the thermal energy, n the electron concentration in the conduction band of the semiconductor photoanode under illuminated conditions and n_o the electron concentration under dark conditions. As it was mentioned previously, due to the increase in charge transfer efficiency in citric acid-treated QDSSCs, more electron accumulation in the conduction band of TiO_2 could happen. This could result in an increase of n, while the E_{Redox} value remains unchanged due to the same electrolyte used in all the above solar cells. Therefore, V_{OC} is clearly expected to be improved when citric acid is used as the linker molecule of QDSSCs [38]. Z_w is related to the finite Warburg impedance which originates from the difference of the diffusion coefficients of the positive and negative ions in the electrolyte as well as the non-blocking character of the electrodes [3,4]. The high value of Z_w of the device with acid-treated photoanode indicates that the oxidation and reduction reactions might be faster in the device than the QDSSC with untreated photoanode as observed by Kim *et al* [43]. Therefore, EIS data are consistent with the increase in the

efficiency due to the enhancement in both the J_{SC} and V_{OC} of the citric acid-treated QDSSC. To show the above charge transfer process within the device, band positions and possible charge transfer mechanism are schematically shown in figure 10 [44]. As it is well-known that when the QDSC are exposed to the sunlight, the QDs harvest some photon energy in the light corresponding to their band gap values. Accordingly, in this case; CdS QDs with 2.3 eV band gap absorb the corresponding photons and generate the photo-excited electrons. These excited electrons are then injected from its conduction band (CB) to the CB of the TiO_2 semiconductor and then, subsequently migrated to the external circuit through the conductive substrate where TiO_2 is deposited (FTO). These electrons then, migrate towards the counter electrode. Meantime, holes produced by the photo-excitation process synchronously in the valence band of the QDs, are immediately transferred to the redox electrolyte to oxidize it. The oxidized electrolyte obtained the electrons in the counter electrode from external circuit in the device. One of the crucial factors determining the overall efficiency is the electron separation and transport before recombining within the device. Therefore, in the present case, since the TiO_2 crystallites are covered with the CA, the back electron transfer from the CB of TiO_2 must be minimized as confirmed by the EIS measurements.

4.   Conclusion

To conclude, we have demonstrated that the citric acid can be used as an efficient capping agent for CdS QDs to largely increase the QD loading of the TiO_2 photoanode and enhance light harvesting, while prompting electron transfer dynamics and suppressing the recombination of separated charges. An overall efficiency as high as 1.5% for the CdS, QD-sensitized solar cell is achieved using this simple strategy. The overall photovoltaic performance of QDSSC with citric acid-linked CdS photoanode showed 36% enhancement over the device fabricated with untreated TiO_2 photoanode. The efficiency enhancement follows the trend observed in the charge transfer studies as well as in the significant enhancement in the current density. The citric acid molecules were well stabilized in the CdS against agglomeration, thereby suppressing the recombination of separated charges.

Acknowledgements

References

[1] Zhang Z, Yang Y, Gao J, Xiao S, Zhou C, Pan D *et al* 2018 *Mater. Today Energy* **7** 27

[2] Zhang Y, Tian J, Jiang K, Huang J, Zhang L, Wang H *et al* 2017 *J. Mater. Sci.: Mater. Electron.* **28** 14103

[3] Dissanayake M A K L, Jaseetharan T, Senadeera G K R, Kumari J M K W, Thotawatthage C A, Mellander B E *et al* 2019 *J. Solid State Electrochem.* **23** 1787

[4] Dissanayake M A K L, Jaseetharan T, Senadeera G K R and Kumari J M K W 2020 *J. Solid State Electrochem.* **24** 283

[5] Chen X, Lan Z, Zhang S, Wu J and Zhang J F 2017 *Opt. Commun.* **395** 111

[6] Du Z, Artemyev M, Wang J and Tang J 2019 *J. Mater. Chem. A* **7** 2464

[7] Zhang D, Ma P, Wang S, Xia M, Zhang S, Xie D *et al* 2019 *Appl. Surf. Sci.* **475** 813

[8] Yang J, Oshima T, Yindeesuk W, Pan Z, Zhong X and Shen Q 2014 *J. Mater. Chem. A* **2** 20882

[9] Hines D A and Kamat P V 2014 *ACS Appl. Mater. Interfaces* **6** 3041

[10] Wang H, McNellis E R, Kinge S, Bonn M and Cánovas M 2013 *Nano Lett.* **13** 5311

[11] Pan Z, Mora-Seró I, Shen Q, Zhang H, Li Y, Zhao H *et al* 2014 *J. Am. Chem. Soc.* **136** 9203

[12] Wang D, Yin F, Du Z, Han D and Tang J 2019 *J. Mater. Chem. A* **7** 26205

[13] Wang J, Mora-Seró I, Pan Z, Zhao K, Zhang H, Feng Y *et al* 2013 *J. Am. Chem. Soc.* **135** 15913

[14] Liu F, Zhu J, Wei J, Li Y, Hu L, Huang Y *et al* 2014 *J. Phys. Chem. C* **118** 214

[15] Aldakov D, Sajjad M T, Ivanova V, Bansal A K, Park J, Reiss P *et al* 2015 *J. Mater. Chem. A* **3** 19050

[16] Margraf J T, Ruland X, Sgobba V, Guldi D M and Clark T 2013 *Langmuir* **29** 2434

[17] Zhang D, Zhang S, Fang Y, Xie D, Zhou X and Lin Y 2021 *Electrochim. Acta* **367** 137452

[18] Pu Y C, Ma H, Sajben N, Xia G, Zhang J, Li Y *et al* 2018 *ACS Appl. Energy Mater.* **1** 2907

[19] Dibbell R S and Watson D F 2009 *J. Phys. Chem. C* **113** 3139

[20] Qian S, Wang C, Liu W, Zhu Y, Yao W and Lu X 2011 *J. Mater. Chem.* **21** 4945

[21] Wei L, Li F, Hu S, Li H, Chi B, Pu J *et al* 2015 *J. Am. Ceram. Soc.* **98** 103173

[22] Razzaq A, Lee J Y, Bhattacharya B and Park J K 2014 *Appl. Nanosci.* **4** 745

[23] Yu L, Li Z and Song H 2017 *J. Mater. Sci.: Mater. Electron.* **28** 2867

[24] Zhang T, Xia Y, Diao X and Zhu C 2018 *J. Nanopart. Res.* **10** 59

[25] Lin S C, Lee Y L, Chang C H, Shen Y J and Yang Y M 2007 *Appl. Phys. Lett.* **90** 143517

[26] Mudunkotuwa I A and Grassian V H 2010 *J. Am. Chem. Soc.* **132** 14986

[27] Chen R, Shao N, Zhou X and Chen T 2020 *Surfaces* **3** 50

[28] Li W, Liang R, Hu A, Huanga Z and Zhou Y N 2014 *RSC Adv.* **4** 36959

[29] Jiang X, Manawan M, Feng T, Qiana R, Zhaoa T, Zhoua G *et al* 2017 *Catal. Today* **300** 1

[30] Saravy H J, Safari M, Khodadadi-Darban A and Rezaei A 2014 *Anal. Lett.* **47** 1772

[31] Wang Z, Xiao X, Zou T, Yang Y, Xing X, Zhao R *et al* 2019 *Nanomaterials* **9** 32

[32] Cao S, Jiao Z, Chena H, Jianga F and Wang X 2018 *J. Photochem. Photobiol. A: Chem.* **364** 22

[33] Kavil J, Alshahrie A and Periyat P 2018 *Nano-Struct. Nano-Objects* **16** 24

[34] Meng Z D, Zhu L, Ye S, Sun Q, Ullah K, Cho K Y *et al* 2013 *Nanoscale Res. Lett.* **23** 189

[35] Sero I M, Likodimos V, Giménez S, Ferrero E M, Albero J, Palomares E *et al* 2010 *J. Phys. Chem. C* **114** 6755

[36] Yang Z, Chen C, Liu C, Li C and Chang H 2011 *Adv. Energy Mater.* **1** 259

[37] Cho S I, Sung H K, Lee S J, Kim W H, Kim D H and Han Y S 2019 *Nanomaterials* **9** 1645

[38] Chen J, Song J L, Sun X W, Deng W Q, Jiang C Y, Lei W *et al* 2009 *Appl. Phys. Lett.* **94** 153115

[39] Green M 2010 *J. Mater. Chem.* **20** 5797

[40] Gopi C V V M, Haritha M V, Seenu R, Tulasivarma C V, Kim S and Ki H 2015 *J. Mater. Chem. C* **3** 12514

[41] Samadpour M, Jun H K, Parand P and Najafi M N 2019 *Sol. Energy* **188** 825

[42] Ranjitha A, Muthukumarasamy N, Thambidurai M, Velauthapillai D R, Balasundaraprabhu R and Agilan S 2013 *J. Mater. Sci.: Mater. Electron.* **24** 3014

[43] Kim H J, Kim D J, Rao S S, Savariraj A D, Kyoung S K, Son M K *et al* 2014 *Electrochim. Acta* **127** 427

[44] Ye M, Gao X, Hong X, Liu Q, He C, Liu X *et al* 2017 *Sustain. Energy Fuels* **1** 1217